Available online at www.sciencedirect.com
SCIENCE DIRECT®
Journal of Sound and Vibration 293 (2006) 38–58
JOURNAL OF SOUND AND VIBRATION
www.elsevier.com/locate/jsvi

Dynamic response of an axially loaded tendon of a tension leg platform

Mangala M. Gadagi, Haym Benaroya*

Department of Mechanical and Aerospace Engineering, Rutgers University, 98 Brett Road, Piscataway, NJ 08854, USA

Received 16 November 2004; received in revised form 29 August 2005; accepted 21 September 2005
Available online 1 December 2005

Abstract

In this work, a set of nonlinear equations of motion for a coupled axial and transverse vibration of a tower subjected to end tension is derived using Hamilton's principle. The in-plane fluid forces are represented by the Morison equation. The tower is modeled as an elastic beam subjected to end tension with only in-plane motions due to random wave loadings. The dynamic response of the tower is analyzed for various end tensions by the finite difference method. The effects of parameter variations such as an increase in significant wave height, an increase in the constant end tension, and harmonically varying end tension are analyzed both for a reduced model and for an actual tether.

It was observed that at low tension, the axial motion is mainly induced by geometry while at higher tension, the axial motion is mainly due to elongation. Analysis of a 260 m tendon showed that increasing the significant wave heights increased the amplitude of transverse response, while the magnitude of axial response remained almost the same. The bending stress in the tendon decreases with an increase in tension due to decreased transverse displacement, but the total stress in the tendon increases with an increase in end tension. The magnitude of transverse displacement could be kept within specific limits by constantly varying the end tension.

1. Introduction

Due to urbanization, the production and consumption of oil and other petroleum products have been rapidly increasing over the years. This has led to the scarcity of easily retrieved oil. As a result, oil producers are motivated to go to deeper ocean to extract oil and other resources. This interest in deep water drilling has led to the in-depth study and analysis of deep water structures, like the Tension Leg Platform (TLP), that are more adaptive to deep waters [1]. TLPs are compliant structures consisting of a pontoon, columns and a deck, and are vertically moored at each corner by tendons. Each tendon is pre-tensioned so that it does not go slack due to variations in the extreme ocean environment. A schematic diagram of a typical TLP is shown in Fig. 1.

A large number of TLPs have been built in the Gulf of Mexico in recent years. The tension in the tendons is a function of the environmental conditions under which the structure must operate. TLPs are available for use in water depths of up to 6000 ft. An example is Anadarko's TLP in the Marco Polo field in the Gulf of Mexico.

*Corresponding author. Tel.: +732 445 4408; fax: +732 445 3124.
E-mail address: benaroya@rci.rutgers.edu (H. Benaroya).

0022-460X/$ - see front matter © 2005 Elsevier Ltd. All rights reserved.
doi:10.1016/j.jsv.2005.09.027

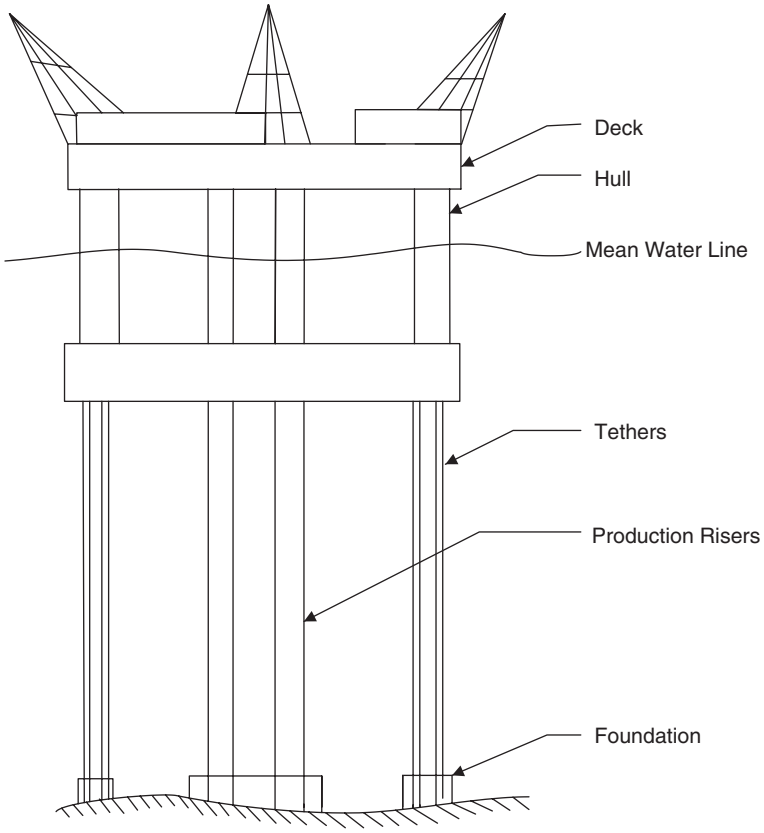

Fig. 1. Schematic diagram of tension leg platform.

It is the deepest TLP in the world at 1311 m (4300 ft) water depth and is designed to process 120,000 barrels of oil and 400 million cubic feet of natural gas per day. The project cost was approximately $210 million.

Due to such huge investments, there is interest in the study of the dynamic responses of such structures under various loads, leading to improved performance and increased design lives.

The dynamic response of offshore structures is a very complex phenomenon. They are governed by equations of motion that are highly nonlinear and depend on both time and space. Study of such structures often begins by idealization, using beam models of various sophistication subjected to waves and other loadings. Some studies are based on the simplest single-degree-of-freedom (dof) model that assume the coupling between the transverse and axial motion to be negligible, while a majority of the studies are more general. Due to a wide variety of applications in engineering, the transverse vibration of beams subjected to axial loads has been studied in depth.

Bokaian [2,3] studied the effect of a constant axial force on natural frequencies and mode shapes of a uniform single-span beam. Luo [4] investigated the eigenproperties of the lateral vibration of an axially loaded infinite beam subjected to a harmonically varying concentrated transverse force at the center.

Jain [5] analyzed the dynamic response of a TLP to deterministic first-order wave forces. The study involved the response due to varying tension in the cable produced by hydrodynamic drag forces. Parametric studies were performed for different values of pretension and it was concluded that the natural period for surge, sway and yaw did not cause resonance as it was well above the natural frequency of external loads. The heave frequency of oscillations of the TLP, however, was close to that of the frequently occurring wave frequency, leading to large tension in the tether and the possibility of resonance. It was observed that the heave motion, although small, was not insignificant and the fluctuation of tether tension was of much concern from the fatigue point of view. Neglecting the coupling between various degrees of freedom could lead to a highly underestimated heave response.

Ahmad [6] studied the coupled responses of TLPs under the influence of random waves in long crested seas retaining the nonlinearities due to drag force, variable submergence, large deformation and randomly varying tether tension. The study showed that one of the factors that influences the overall response is the pretension in the tethers. The heave response and the tether tension are critically affected by the coupling between degrees of freedom. Instantaneous fluctuations in tether tension are a source of nonlinearity and are of great concern from the fatigue point of view. Variable submergence causes fluctuations in the axial force of the tether, thus contributing to the nonlinearity of TLP dynamics and significantly increasing the surge and heave responses.

Takahashi and Konishi [7] studied the nonlinear vibration of both horizontal and inclined sagged cables supported at the ends. They observed that the cable behaved like a hardening spring in the case of nonlinear free vibration.

Triantafyllou and Howell [8] showed that the dynamics of a perfectly elastic linear or nonlinear cable constituted an ill-posed problem when the tension becomes negative at any point along the cable. To change the system to a well-posed problem, the bending stiffness has to be included in the analysis even if it is very small.

Virgin and Plaut [9] studied the effects of static axial loads on the forced vibration of a beam by subjecting it to a harmonically varying transverse distributed load. Their study revealed that as the axial load increases, the resonant amplitude of the central deflection increases and the corresponding resonant forcing frequency decreases. The response amplitude grew quickly as the axial load approached the buckling load.

Dong et al. [10] investigated the vortex-induced transverse nonlinear oscillation of a tether by subjecting it to parametric excitation of a frequency equal to the natural frequency of the system. The equation of motion of a single dof nonlinear model was used. It was observed that the system became unstable for small values of the damping and lift coefficients. For moderate damping and lift coefficients, there were multiple equilibrium positions, and for sufficiently large values of the coefficients, the regions of multiple solutions vanish. The stable solution of the system converges to a limit cycle. The beating phenomenon increases with the detuning parameter, but chaotic behavior was not observed.

In order to understand the three-dimensional response of the TLP in a better way, Han and Benaroya [11] modeled the structure both as a rigid body and as an elastic member and compared their dynamic responses. The study revealed that the fundamental frequency of response obtained from both models matched, and rotating elliptical paths were observed when viewed from the top. The elastic model showed subharmonics of order 1/2 and 1/3 when the transverse force is applied in only one direction. The displacement in the perpendicular direction remained almost unaffected. A comparison of linear and nonlinear responses of a compliant tower to random waves was done by Han and Benaroya [12].

Mekha et al. [13] explored the implications of tendon modeling on the overall response of TLPs. Three different models of tendons were used: the first, a massless elastic spring with constant lateral stiffness, the second, an elastic spring with time-varying axial forces and one-third of tendon mass lumped at the point of attachment, and the last one, a flexural beam with time-varying axial forces. Their study showed that the amplitude of the surge motion varied linearly with significant wave height but was not affected by the nonlinearity due to varying axial forces or by water depth, and so the simplest model can be used if only the surge motion amplitude is to be predicted. It was also shown that the mean horizontal drift was influenced by the variations in the hydrodynamic forces, wave height and water depth of tendon but was unaffected by variations in the tendon axial forces. All three models showed that the tendon forces varied linearly with the wave height, wave frequency and water depth.

Patel and Park [14] investigated the combined axial and transverse response of tethers of a tensioned buoyant platform. The tether is modeled as a simply supported beam under the action of combined axial and lateral forces. In addition, TLP tethers at low tensions were studied by Patel and Park [15]. It was concluded that the mean tension in the tethers could be decreased to increase the payload over the conventional design of TLP by using the Mathieu stability charts.

Another paper by Patel and Park [16] dealt with the tether response to short duration tension loss. The governing equations of tether lateral motion for short-term tension loss were derived and solved both numerically and analytically to obtain an envelope of compressive axial loads against the duration of its action. This information was used to maintain acceptable levels of stress in the tether under all circumstances.

Their study showed that the tether could be designed to withstand a momentary tension loss due to extreme sea conditions.

Han and Benaroya [17] analyzed the free response of a compliant structure in vacuum and water. Hamilton's principle was used to derive the equations of motion and the corresponding boundary conditions. The transverse and axial responses were nonlinearly coupled. The study revealed that the fundamental frequency of axial motion was twice that of the corresponding value of the fundamental frequency of transverse motion, and this was geometrically induced. It was also found that due to the nonlinear coupling between the axial and transverse displacements, the fundamental frequency of vibration varies with the initial condition. In another paper [18], the forced response of the same structure was analyzed.

The work of Han and Benaroya are the basis of current study. In their earlier work [17,18], they derived the nonlinear coupled equations of motion and analyzed the response for various cases of loadings. However, their study did not include the end tension in the analysis. In the current study, a set of nonlinear equations of motion for a coupled axial and transverse vibration of a tether subjected to end tension is derived using Hamilton's variational approach. The in-plane fluid forces are represented by the Morison equation. The random waves are characterized by the Pierson–Moskowitz power spectrum and are converted to time domain using Borgman's method. The equations of motion are solved numerically using a finite difference method. The influence of tension on the dynamic behavior of the structure is analyzed. How the structure responds to changes in end tension, and the variation of the stress occurring in the tether due these changes, are studied here.

2. Mathematical formulation: coupled axial and transverse vibration with end tension

Much work has been done on the subject of transverse vibration of beam with axial forces. The general formulation for such a problem is studied in Refs. [19–21]. The purpose of this study is to explore the coupled axial and transverse vibration of the tower with applied end tension. Fig. 2 shows a simplified model of a single tether of a TLP. The tower is modeled as an elastic beam with length L and mass M at its free end. It is assumed to be extensible and confined only to the x–y plane. It has a linear elastic torsional spring with a spring constant K at the lower end and is subjected to an applied tensile force $F_t(x,t)$ at the upper end. The in-plane transverse load is due to the waves and is approximated using the Morison equation. The equations of motion and the corresponding boundary conditions are derived using Hamilton's variational approach. The response of the tower is analyzed under various tensions (see Table 1 for a list of nomenclature).

The total kinetic energy of the system T_{sys} is due to the kinetic energy of the beam T_{beam} and that of the point mass T_m. This is composed of the translational kinetic energy and the rotational kinetic energy,

$$T_{\text{sys}} = \frac{1}{2}\int_0^L \rho A((\dot{u}^2+\dot{v}^2)+\rho I(\dot{v}')^2)\,\mathrm{d}x + \frac{1}{2}M_p(\dot{u}^2(L,t)+\dot{v}^2(L,t)),$$

where u is the axial displacement and v the transverse displacement.

The strain energy of the system is due to the elastic deformation of the beam and the rotation of the torsional spring at the base of the tower,

$$V_{\text{beam}} = \frac{1}{2}\int_0^L \left\{ EA(x)\left[u' + \frac{1}{2}(v')^2\right]^2 + EI(x)[v''(x,t)]^2 \right\}\mathrm{d}x.$$

The strain energy stored in the spring is given by

$$V_s = \tfrac{1}{2}K\theta^2,$$

where θ is the angle of twist of the spring. By the small angle approximation, the angle of twist can be approximated by the first spatial derivative of the transverse deflection, $v'(x,t)$. Then,

$$V_s = \tfrac{1}{2}K[v'(x,t)]^2|_{x=0} = \tfrac{1}{2}K[v'(0,t)]^2.$$

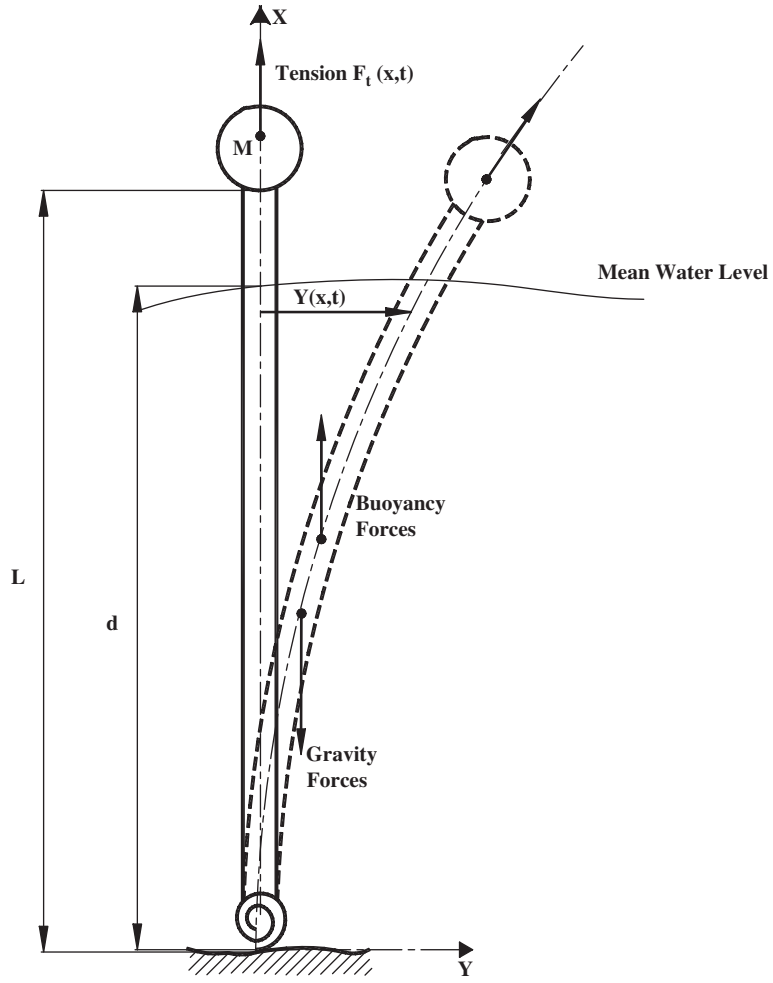

Fig. 2. Schematic diagram of tower with end tension.

The total strain energy is then obtained by adding the two equations:

$$V_{\text{sys}} = \frac{1}{2}\int_0^L \left\{ EA(x)\left[u' + \frac{1}{2}(v')^2\right]^2 + EI(x)[v''(x,t)]^2 \right\} \mathrm{d}x + \frac{1}{2}K[v'(0,t)]^2.$$

The Lagrangian of the system is then

$$\begin{aligned} L_{\text{sys}} &= T_{\text{sys}} - V_{\text{sys}} \\ &= \frac{1}{2}\int_0^L \left[\rho A(\dot{u}^2 + \dot{v}^2) + \rho I(\dot{v}')^2 - EA(x)\left[u' + \frac{1}{2}(v')^2\right]^2 \right. \\ &\quad \left. -EI(x)[v''(x,t)]^2 \right] \mathrm{d}x + \frac{1}{2}M_p[\dot{u}^2(L,t) + \dot{v}^2(L,t)] - \frac{1}{2}K[v'(0,t)]^2. \end{aligned}$$

2.1. Generalized forces

In this section, the generalized forces acting on the system are obtained. In an ocean environment there are a number of forces acting on the tower, such as the force due to wave, wind, current, wave slamming, among

Table 1
Nomenclature

Symbol	Description	Units
d	Depth of water	m
$f_t(x,t)$	Transverse fluid force	N
g	Acceleration due to gravity	m/s^2
t	Time	s
u	Axial tower displacement	m
$\dot{u}$	Axial tower velocity	m/s
v	Transverse tower displacement	m
$\dot{v}$	Transverse tower velocity	m/s
W_x	Wave velocity in x direction	m/s
W_y	Wave velocity in y direction	m/s
A_t	Tower cross-section area	m^2
A_f	Cross-section of the displaced volume of the fluid	m^2
C_a	Added mass coefficient	dimensionless
C_d	Drag coefficient	dimensionless
C_m	Inertia coefficient	dimensionless
D_i	Inner diameter of the tower	m
D_o	Outer diameter of the tower	m
E	Young's modulus	Pa (N/m^2)
F_t	Tensile force along beam axis	N
H_s	Significant wave height	m
I_z	Moment of inertia about the z-axis	m^4
K	Torsional spring constant	Nm/radian
M_p	End mass	kg
θ	Angle of twist of the spring	Radians
ρ_t	Density of the tower	kg/m^3
ρ_f	Fluid density	kg/m^3
ω	Frequency	rad/s
σ	Stress	N/m^2

other forces. In this study only the forces due to waves are considered. As the diameter of the cylinder is small compared to the wavelength of the incident wave, Morison's equation is used to model the in-plane fluid forces per unit length [22]. If $Q(x,t)$ and $P(x,t)$ represent generalized transverse and longitudinal forces, respectively, then the virtual work is given as

$$\delta w = \frac{1}{2}\int_0^L [Q(x,t)\delta v + P(x,t)\delta u]\,\mathrm{d}x,$$

where δu and δv represent the virtual longitudinal and transverse displacements, respectively.

The generalized longitudinal force $P(x,t)$ is due to gravity, buoyancy, and the tensile force acting along the axis,

$$P(x,t) = p(x,t) + F_t(x,t),$$

where

$$\begin{aligned} p(x,t) &= (\rho_f A_f - \rho A_t)g \quad \text{for } 0 < x \leqslant d, \\ &= -\rho A_t g \quad \text{for } d < x \leqslant L. \end{aligned}$$

A_f represents the area of fluid displaced by the tower, A_t represents the area of tower and $F_t(x,t)$ represents the tensile force along the axis. These forces are assumed to be always acting along the axis of beam element due to the small angle assumption (Fig. 3).

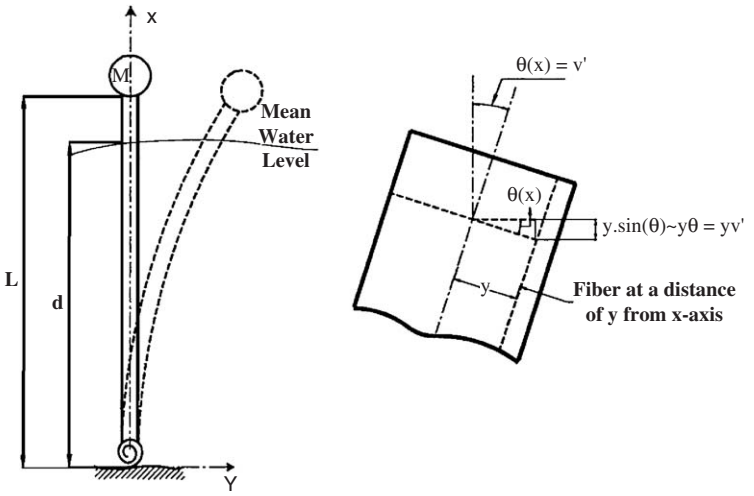

Fig. 3. Element at a distance of Y from the neutral axis.

The transverse generalized forces $Q(x,t)$ acting on the system in an ocean environment is represented by the Morison equation,

$$Q(x,t) = \tfrac{1}{2}C_d\rho_f D_o(W_y + \dot{u}v' - W_x v' - \dot{v})|W_y + \dot{u}v' - W_x v' - \dot{v}| + \tfrac{1}{4}C_m\pi\rho_f D_o^2(\dot{W}_y - \dot{W}_x v') - \tfrac{1}{4}C_a\pi\rho_f D_o^2(\ddot{v} - \ddot{u}v'), \quad (1)$$

where W_y and W_x are the wave velocities in y and x directions, $\dot{W}_y$ and $\dot{W}_x$ are the wave accelerations in y and x directions, C_d is the drag coefficient, C_m is the inertia coefficient, C_a is the added mass coefficient, ρ_f is the fluid density, and D_o is the outer diameter of the tower. Note that the relative velocity between the fluid and the tower is considered here. Structural damping is not used in the analysis.

The wave velocities are determined using random wave theory, and characterized by the Pierson–Moskowitz power spectrum, as described by Chakrabarti [23] and converted to the time domain using Borgman's method. It can be shown that the wave velocities are given by

$$W_y(x,y,t) = \frac{H_s}{4}\sqrt{\frac{2}{P}}\sum_{p=1}^{P}\bar{\omega}_p\frac{\cosh\,\bar{k}_p x}{\sinh\,\bar{k}_p d}\cos(\bar{k}_p y - \bar{\omega}_p t + \Delta), \quad (2)$$

$$W_x(x,y,t) = \frac{H_s}{4}\sqrt{\frac{2}{P}}\sum_{p=1}^{P}\bar{\omega}_p\frac{\sinh\,\bar{k}_p x}{\sinh\,\bar{k}_p d}\sin(\bar{k}_p y - \bar{\omega}_p t + \Delta), \quad (3)$$

where H_s is the significant wave height, Δ is the random phase angle between 0 and 2π, and

$$\bar{\omega}_p = \frac{\omega_p + \omega_{p-1}}{2}, \quad \bar{k}_p = k(\bar{\omega}_p) \quad \text{for } p = 1,\ldots,P.$$

ω_p represents the pth angular frequency, k_p is the pth wavenumber. The zeroth frequency ω_0 equals zero, and ω_P is chosen so that most of the area under the Pierson–Moskowitz spectrum is contained between ω_0 and ω_P. The frequencies in between, that is, ω_1 to ω_{P-1}, are chosen such that there is equal area under each segment of the spectral curve [24]. Therefore, ω_p is given by

$$\omega_p = \left(\frac{B}{\ln(P/p) + (B/\omega_p^4)}\right)^{1/4} \quad \text{for } p = 1,\ldots,P-1,$$

where B is a constant and is defined in terms of the significant wave height,

$$B = \frac{4A_o}{H_s^2},$$

$A_o = 0.0081g^2$, and g is the acceleration due to gravity.

The wave accelerations are obtained by taking the time derivatives of Eqs. (2) and (3),

$$\dot{W}_y(x,y,t) = \frac{H_s}{4}\sqrt{\frac{2}{P}}\sum_{p=1}^{P}\bar{\omega}_p^2\frac{\cosh(\bar{k}_p x)}{\sinh(\bar{k}_p d)}\sin(\bar{k}_p y - \bar{\omega}_p t + \Delta),$$

$$\dot{W}_x(x,y,t) = -\frac{H_s}{4}\sqrt{\frac{2}{P}}\sum_{p=1}^{P}\bar{\omega}_p^2\frac{\sinh(\bar{k}_p x)}{\sinh(\bar{k}_p d)}\cos(\bar{k}_p y - \bar{\omega}_p t + \Delta).$$

These velocities and accelerations are substituted into Eq. (1) for the generalized transverse force.

2.2. Equations of motion and the boundary conditions

Once the Lagrangian has been formulated and the virtual work determined, these are substituted into Hamilton's principle and varied,

$$\delta\int_{t_1}^{t_2} L_{\text{sys}}\,\mathrm{d}t + \int_{t_1}^{t_2}\delta W\,\mathrm{d}t = 0,$$

$$\begin{aligned}\delta\frac{1}{2}\int_{t_1}^{t_2}\int_0^L\left[\rho A(\dot{u}^2+\dot{v}^2)+\rho I(\dot{v}')^2 - EA\left[u'+\frac{1}{2}(v')^2\right]^2 - EI[v'']^2\right]\mathrm{d}x\,\mathrm{d}t\\ +\frac{1}{2}\delta\int_{t_1}^{t_2}\left[M_p[\dot{u}^2(L,t)+\dot{v}^2(L,t)]-\frac{1}{2}K[v'(0,t)]^2\right]\mathrm{d}t\\ +\frac{1}{2}\int_{t_1}^{t_2}\int_0^L[Q(x,t)\delta v + P(x,t)\delta u]\,\mathrm{d}t = 0.\end{aligned}$$

This can be simplified by assuming uniform beam properties, and applying the condition that the variations at the end times are zero, we obtain the two nonlinear coupled governing equations of motion,

$$\rho A\ddot{u} - [EA_t(u' + \tfrac{1}{2}(v')^2)]' = P(x,t), \tag{4}$$

$$\rho A_t\ddot{v} - [EA_t(u' + \tfrac{1}{2}(v')^2)v']' - \rho I(\ddot{v}')' + [EIv''(x,t)]'' = Q(x,t), \tag{5}$$

with the corresponding general boundary conditions

$$M_p\ddot{u}(L,t)\delta u + EA(u' + \tfrac{1}{2}(v')^2)\delta u|_0^L = 0, \tag{6}$$

$$[[EIv'']' - \rho I\ddot{v}' - EA_t(u' + \tfrac{1}{2}(v')^2)v']\delta v|_0^L - M_p\ddot{v}(L,t)\delta v = 0, \tag{7}$$

$$EIv''(x,t)\delta v'|_0^L + Kv'(0,t)\delta v'(0,t) = 0. \tag{8}$$

Primes denote partial derivatives with respect to x, and overdots denote partial derivatives with respect to t.

For the problem being considered, the tower is uniform, elastically restrained at $x = 0$, and free at $x = L$, thus, the boundary conditions reduce to

$$u(0,t) = 0, \quad v(0,t) = 0, \tag{9,10}$$

$$Kv'(0,t) - EIv''(0,t) = 0, \tag{11}$$

$$|M_p\ddot{u} + EA_t(u' + \tfrac{1}{2}(v')^2)|_{X=L} = 0, \tag{12}$$

$$|EIv''' - \rho I\ddot{v}' - EA_t(u' + \tfrac{1}{2}(v')^2)v' - M_p\ddot{v}|_{X=L} = 0, \tag{13}$$

$$EIv''(L,t) = 0. \tag{14}$$

The first two boundary conditions imply that the lower end of the beam ($x = 0, y = 0$) has no transverse or longitudinal displacements. The third boundary condition states that the moment at the restrained end is

resisted by the torsional spring, of spring constant K. The fourth and fifth boundary conditions express the force balance in the transverse and longitudinal directions, respectively. The last boundary condition implies that the beam cannot resist a moment at $x = L$.

Similar equations of motion and boundary conditions are obtained by Yigit and Christoforou [25], and Han and Benaroya [24].

3. Numerical results and discussions

Equations of motion (4) and (5), and boundary condition (9–14), are discretized using a second-order central difference approximation. The length of the tower L is divided by N nodes placed at equal distances $h = L/N$ along its length with the first node at $X = h$ and the Nth node is at $X = L$. This yields a system of $2N$ second-order differential equations. Each of these in turn is expressed as two first-order differential equations, resulting in a system of $4N$ first-order ordinary differential equations. The general equation of central difference method gives

$$v''(n) = [v(n+1) - 2v(n) + v(n-1)]/2h.$$

So,

$$v''(0) = [v(1) - 2v(0) + v(-1)]/2h,$$

$$\begin{aligned} 0 &= [v(1) - 2v(0) + v(-1)]/2h \\ &= [v(1) - 0 + v(-1)]/2h \end{aligned}$$

and $v(-1) = v(1)$. By the same method the values of the fictitious nodes at the other boundary ($x = L$) can be evaluated.

The system is solved for the independent variables using MATLAB, applying the appropriate initial conditions.

4. Response of a 1.27 m beam model to various end tensions

The beam is taken to have zero initial conditions, implying that it is initially straight and upright, and has no initial velocity. Fourteen nodes are used for the computational model. The properties of the system are given in Table 2. The hollow tower is composed of aluminum, to match the properties of an in-house experiment. The values of the inertia coefficient C_m and the drag coefficient C_d represent the average value encountered in practice. The tower is subjected to random wave loads in the transverse direction. The peak angular frequency ω_{peak} of the Pierson–Moskowitz spectrum is 2 rad/s, which corresponds to a significant wave height of $H_s = 0.3957$ m.

Table 2
Beam and fluid properties

Parameters	Values
ρ_t	2770 kg/m^3
ρ_f	999 kg/m^3
D_o	0.0254 m
D_i	0.022 m
L	1.27 m
E	73×10^9 Pa
d	1.05 m
C_m	1.5
C_d	1
C_a	1
H_s	0.3957 m
σ_{yield}	96.5×10^6 Pa

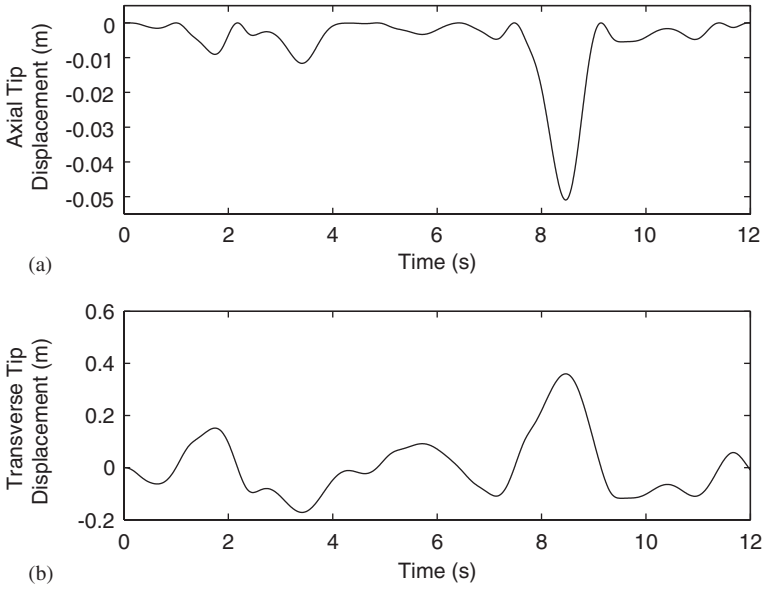

Fig. 4. Response of the tower with zero end tension: (a) axial tip displacement, (b) transverse tip displacement.

Fig. 4 shows the response of the tower with no end tension. The maximum transverse displacement is 0.3598 m and the maximum absolute axial displacement is 0.0510 m. The maximum stress in the tower is 13.35 MPa. The response of the tower is then analyzed for different values of tension. The tower is subjected to constant values of tension that are multiples of the buoyancy force B : $5B, 10B, 15B, 20B, 25B, 30B, 35B, 50B$ and $100B$.

The overall trace of the response remains similar, but both the transverse and the axial displacements decrease as the tension is increased. When there is no tension, the axial displacement is mainly induced due to geometry. As the tension increases, the geometrically induced axial displacement decreases. Further increase in tension causes the axial displacement to be mainly due to elongation. Also, the frequency of axial vibration increases from 0.1464 to 0.1953 Hz as the tension increases from $0B$ to $100B$. This increase in frequency is expected with an increase in the end tension. Figs. 5 and 6 show that for very large tensions, there is a very high frequency oscillation superimposed on the larger motion.

From Table 3, it is observed that the maximum stress is 13.35 MPa when there is no tension. As the transverse displacement is large, the bending stress in the tower is large, which contributes to higher maximum stress. As the tension is increased, the maximum stress occurring in the tower initially decreases. This is because an increase in tension causes a decrease in transverse displacement, resulting in smaller bending stress, and hence smaller total stress. It can be seen from Table 3 that when the tension in the tower is $30B$, the maximum tension in the tower has started to increase. The reason for this is that although the bending stress is reduced due to a decrease in transverse motion, larger tension in the tower causes larger axial stress, increasing the total stress occurring in the beam.

4.1. Response of a 260 m tether to wave loading

In this section, the response of a TLP model with structural properties listed in Tables 4 and 5 are presented. These values are based on the technical report *Guidelines for Offshore Structural Reliability Analysis* [26]. The TLP model has four columns and pontoons supported by four tethers at each corner. It has a total displacement of 200,000 tons. The mean water depth is 325 m. In the current study, the response of one of the tethers subjected to random wave loads is analyzed. The total tether pretension is 25,000 tons. As there are a total of 16 tethers, the displacement and the pretension are assumed to be equally distributed to each tether.

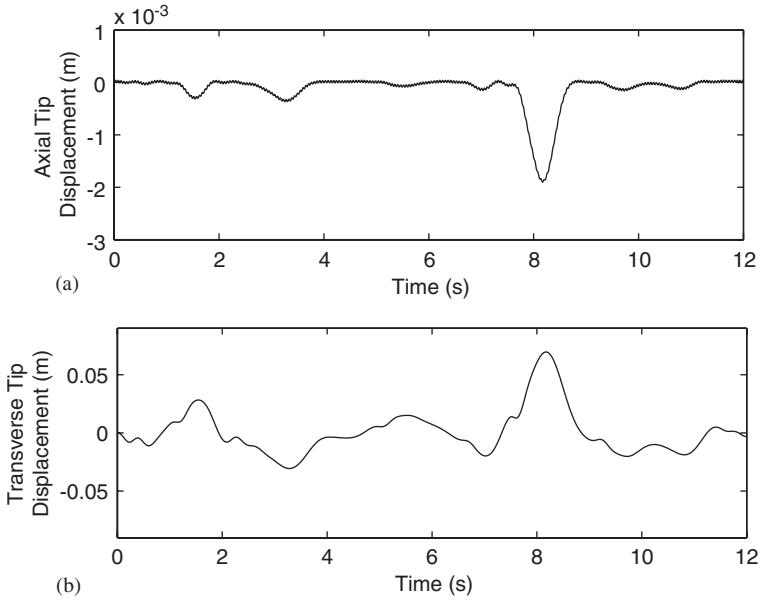

Fig. 5. Response of the tower with end tension $T = 50B$: (a) axial tip displacement, (b) transverse tip displacement.

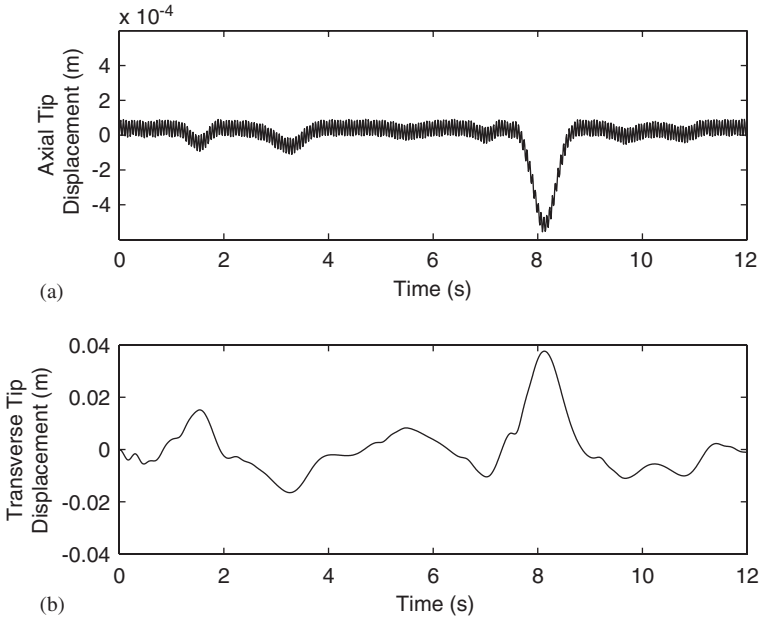

Fig. 6. Response of the tower with end tension $T = 100B$: (a) axial tip displacement, (b) transverse tip displacement.

A representative response of the system to stochastic wave forces with different significant wave heights is shown in Fig. 7. Each tether is subjected to a constant end tension of 1562.5 tons. This end tension is kept constant during the analysis. The figure shows oscillation about the vertical equilibrium position. As can be expected, increasing the significant wave height increases the amplitude of transverse response. This in turn increases the maximum stress occurring in the system. The values of maximum stress for significant wave heights of 9, 12, 15 and 20 m are shown in Table 6.

Table 3
Maximum stresses and displacements for various end tensions

Tension	Maximum stress (MPa)	Maximum absolute axial displacement (m)	Maximum absolute transverse displacement (m)
0*B*	13.35	0.0510	0.3598
5*B*	9.74	0.0260	0.2575
10*B*	8.17	0.0158	0.2002
15*B*	7.17	0.01105	0.1637
20*B*	6.50	0.0075	0.1380
25*B*	6.46	0.0056	0.1190
30*B*	6.51	0.0043	0.1043
35*B*	6.98	0.0034	0.0928
50*B*	7.32	0.0019	0.0696
100*B*	11.7	0.00055	0.0376

Table 4
Dimensions of a tension leg platform

Displacement	200,000 tons
Water depth	325 m
Number of tethers	16
Vertical distance between mean water line to top attachment point of tether	55 m
Center line distance between columns	78 m
Column outer diameter	28.5 m
Draft	60 m
Pontoon breadth	14.25 m
Pontoon height	13.0 m

Table 5
Tether geometry

Length	260 m
Drag diameter	1.0 m
Buoyancy diameter	1.0 m
Tether thickness	0.03 m
Pretension per tether	1562.5 tons
Axial stiffness, *EA*	1.92×10^7 kN
Bending stiffness, *EI*	2.26×10^6 kN m^2
Mass	0.718 tons/m
Spring stiffness, *K*	100 kNm/deg
Horizontal distance from center TLP to top attachment point of tether	69.40 m
Vertical distance between mean water line to top attachment point of tether	55 m
Yield stress	358 MPa

The maximum stress occurring in the tethers is well below the yield stress. Due to the possibility of high fatigue damage in the tethers, the stress in the tethers has to be kept to a minimum. It is found that the transverse displacement increased significantly due to an increase in significant wave heights, but the axial response does not increase substantially. The reason behind this appears to be that a major portion of the axial displacement is caused by tension at the end and only a small portion of it is geometrically induced by transverse motion. As the end tension is kept constant, the axial displacement is not much affected.

Representative power spectral density plots of axial and transverse displacements are shown in Figs. 8 and 9. As can be seen, there are peaks at 3.95 Hz in the axial displacement plot and at 0.0366 Hz in the transverse displacement plot, representing the two fundamental frequencies of vibration.

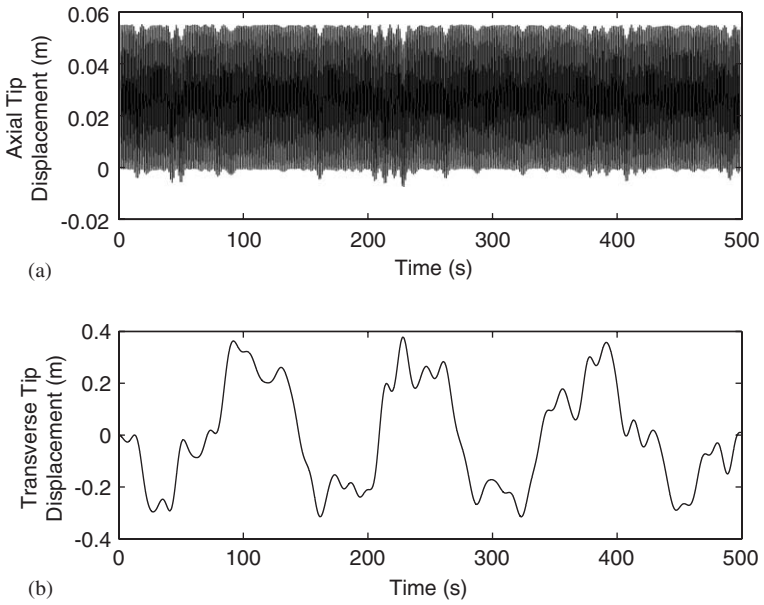

Fig. 7. Tip response to a random wave with significant wave height $H_s = 12\,\text{m}$: (a) axial tip displacement, (b) transverse tip displacement.

Table 6
Maximum stress for different values of significant heights

Significant wave height (m)	Maximum stress (MPa)
9	84.63
12	84.76
15	90.55
20	117.80

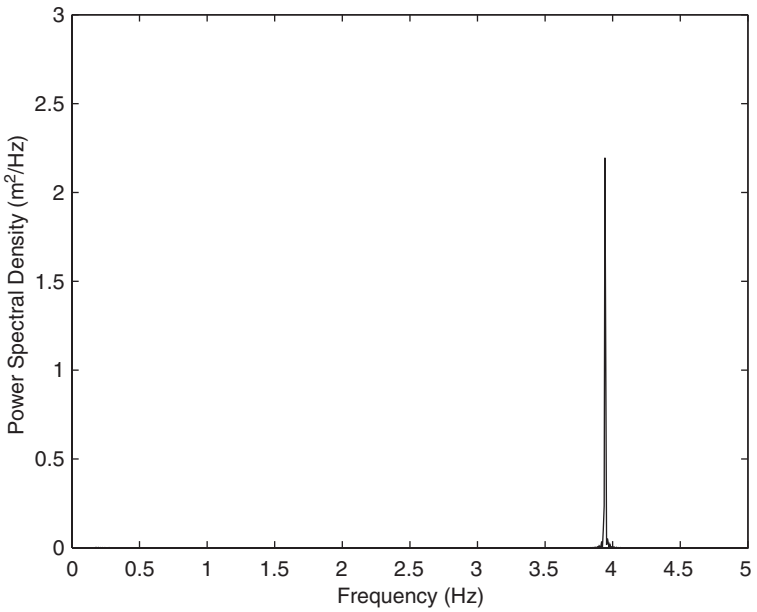

Fig. 8. Power spectral density plot of axial displacement for $H_s = 9\,\text{m}$.

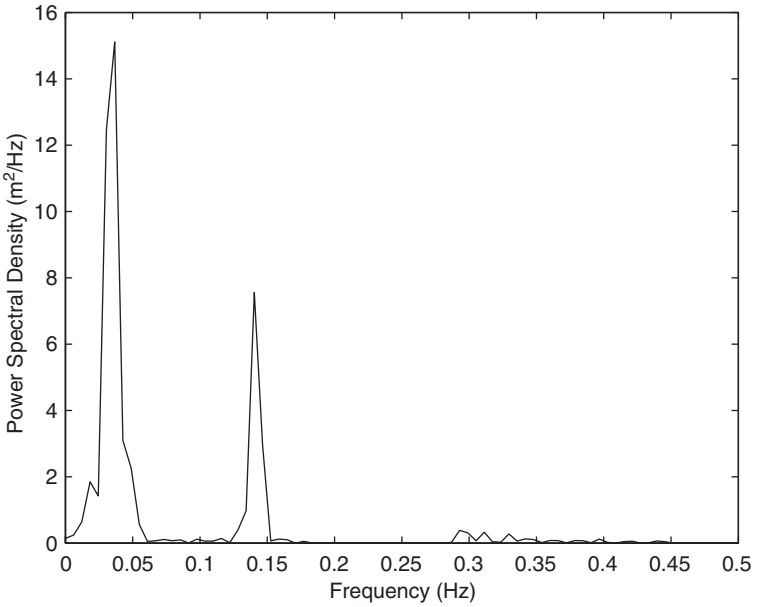

Fig. 9. Power spectral density plot of transverse displacement for $H_s = 9$ m.

4.1.1. Effect of varying the end tension on the response of the tower

The next logical step is to examine the response of the tower for different constant end tensions. The tower is subjected to random waves, with a significant wave height of H_s 15 m. Fig. 10 shows the response of the tower when the end is not subjected to any tension. As such, the axial displacement is mainly induced geometrically and is negative. It is interesting to see that when there is no end tension, the transverse displacements increase with time. This leads to an increase in stress in the structure with time. The maximum bending stress occurring in the structure is 132.82 MPa and the maximum total stress is 136.68 MPa. Clearly, increases in displacement and stress are undesirable in a TLP. One way to decrease this is to increase the end tension.

Next, the tether is subjected to a constant end tension of 1562.5 tons. The significant wave height is kept constant at $H_s = 15$ m to compare the results with previous calculations where the tower was not subjected to any tension. Fig. 11 shows the response of the tower to random wave loads. As expected, the number of transverse oscillation cycles is more for a tether under tension than without tension. Due to the constant end tension, there is elongation of the tether and the axial displacement is mainly positive. The absolute values of the axial and transverse displacements decrease as tension increases. This is because an increase in tension causes an increased bending stiffness that reduces the transverse displacements and hence the axial displacements.

From Fig. 11 it can be seen that when tension in the tether is 1562.5 tons, the maximum transverse displacement is 0.8495 m and the maximum axial displacement is 0.0551 m. The number of cycles of transverse displacement in 2000 s is about 16 and the number of cycles of axial displacement is about 1578 for the same duration. The maximum stress in the tether is 90.53 MPa and the maximum bending stress is 45.49 MPa.

To better understand the effect of tension, the same model is subjected to different constant end tensions. When the tension is increased to 3125 tons, which is twice the initial pretension, the maximum transverse displacement is reduced to 0.3884 m. This is because increasing the tension increases the stiffness and helps to reduce the transverse displacements. The maximum axial displacement almost doubled when the value of the end tension is doubled. This is because higher tension leads to larger axial stretch, which in turn leads to larger axial displacement. The number of cycles of transverse displacement in 2000 s increased to about 47 while the number of cycles for axial displacement remained approximately the same as before. The maximum stress in the tether increased to 163.58 MPa.

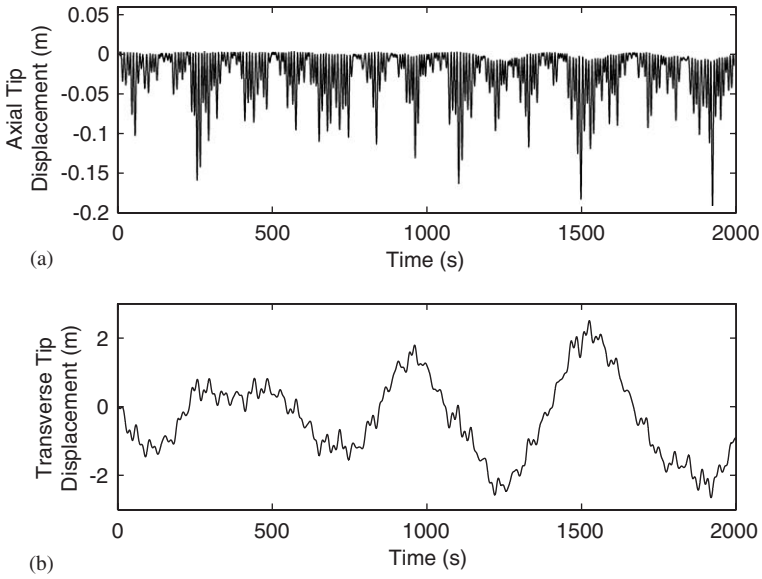

Fig. 10. Tip response to a random wave with significant wave height $H_s = 15$ m and zero end tension: (a) axial tip displacement, (b) transverse tip displacement.

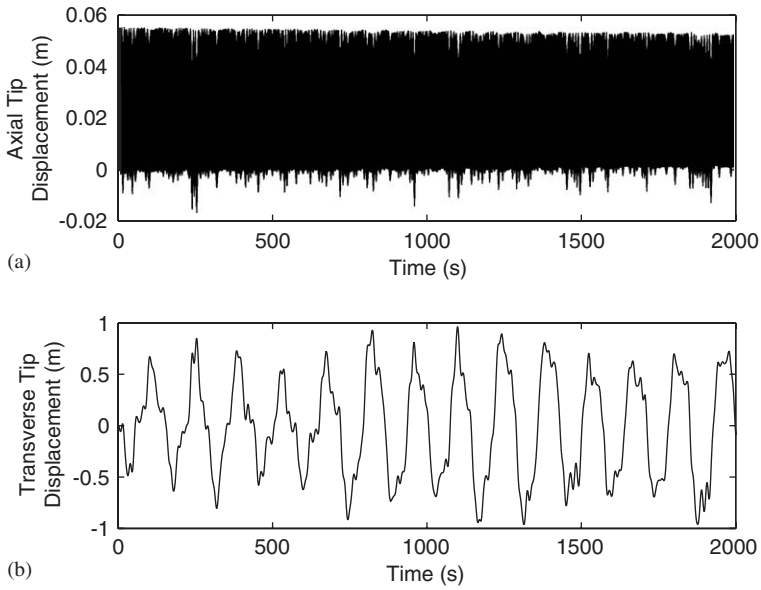

Fig. 11. Tip response to a random wave with a significant wave height $H_s = 15$ m and an end tension of 1562.5 tons: (a) axial tip displacement, (b) transverse tip displacement.

The maximum bending stress and the maximum total stress occurring in the tether is tabulated for several cases in Table 7. In all the cases, the maximum total stress is below the yield stress, which is 358 MPa. It is observed that at low tension, the axial stress in the tether is low and the bending stress is very high, resulting in large total stress. As the tension increases to 1562.5 tons, the axial stress in the tether increases slightly, whereas the bending stress in the tether decreases to a large extent, leading to decreased total stress. With further increase in tension, although there is reduction in the bending stress due to reduced transverse displacement, the total stress in the tether starts to increase due to large axial stress. This can be seen from the last two cases in Table 7.

Table 7
Variation of bending stress and total stress for various end tensions

Tension (tons)	Maximum bending stress (MPa)	Maximum total stress (MPa)
0	132.82	136.68
1562.5	45.49	90.53
3125	31.69	163.56
4687.5	31.10	242.88

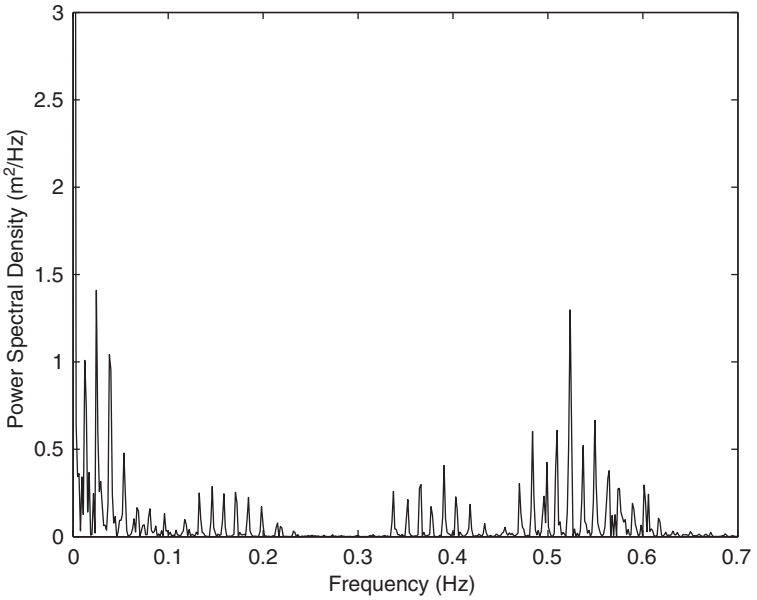

Fig. 12. Power spectral density of axial displacement for zero end tension.

Figs. 12 and 13 show representative power spectral density plots of the axial displacement. As can be seen from Fig. 12, when there is no tension, the peaks occur at lower frequencies. As the tension in the tether increases, the peaks shift to the right, that is, peaks occur at higher frequencies. There is a consistent peak at about 4 Hz for tethers with tension, corresponding to the fundamental frequency of axial response.

The spectral density plots of the transverse displacements also show that as the tension increases, the peaks occur at higher frequencies. This was expected as higher tension in beams result in higher sets of frequencies. Figs. 14 and 15 show representative power spectral densities of transverse displacement.

4.1.2. Response of the tower to varying end tension

Sometimes it is desirable to restrict the transverse displacement of the tower within a particular limit. This can be achieved by either increasing the constant end tension or by constantly varying the tension with time depending on the feedback from the transverse position of the tower tip. One drawback of increasing the end tension in the tether is that it leads to higher total stresses. Larger tension increases the chances of failure of the tether by elongation.

Initially the tether is subjected to a constant end tension of 1252.5 tons. Depending on the magnitude and slope of the transverse displacement, the tension is either increased or decreased by 5% of the total tension, to lower the transverse tip displacement. Fig. 16 shows the response of the tower to a constantly varying end tension. Fig. 17 shows the tether subjected to a constant end tension of 1252.5 tons. All the parameters except the end tension are kept constant in both analyses. The significant wave height in both cases is $H_s = 15$ m.

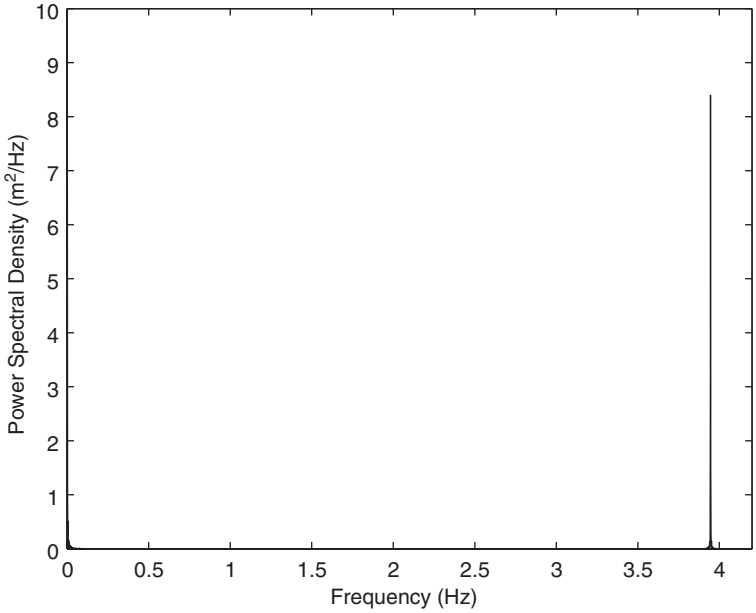

Fig. 13. Power spectral density of axial displacement for 1562.5 tons end tension.

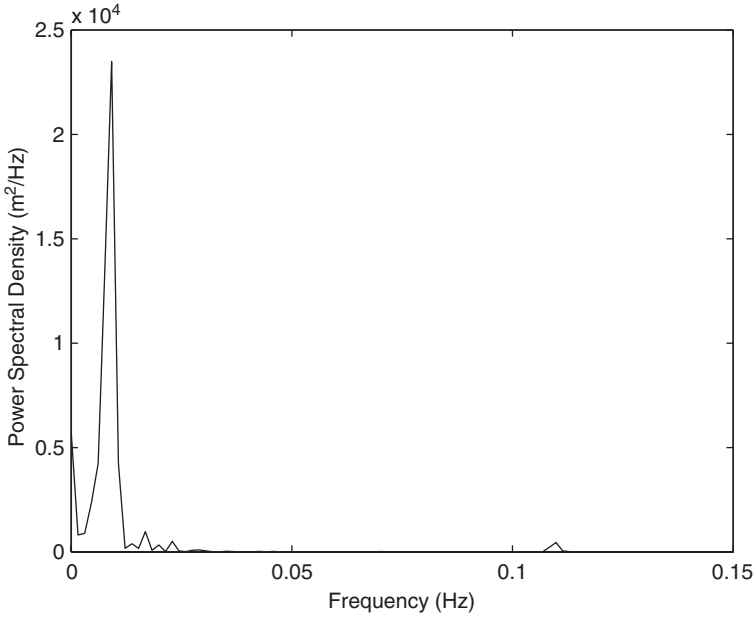

Fig. 14. Power spectral density of transverse displacement for zero end tension.

It can be seen from Fig. 16 that by varying the end tension the magnitude of transverse displacement can be kept within the limits of ± 0.6 m, but the magnitude of the axial displacement increases considerably. There is a clear trade-off.

4.1.3. Response of the tower to harmonically varying end tension

Next, the responses of a system to a harmonically varying end tension are analyzed. The end tension is of the form $T(x,t) = T_o - S\cos\omega t$, where T_o is a constant axial tension, S is the time-varying axial force

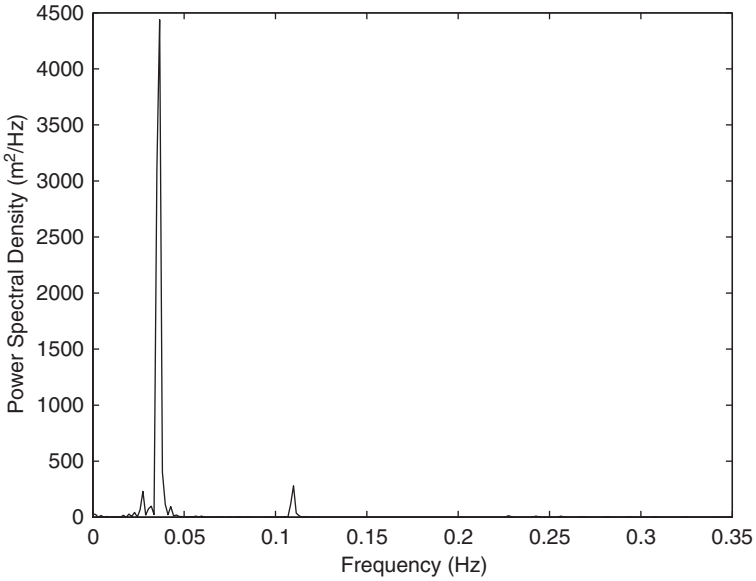

Fig. 15. Power spectral density of transverse displacement for 1562.5 tons end tension.

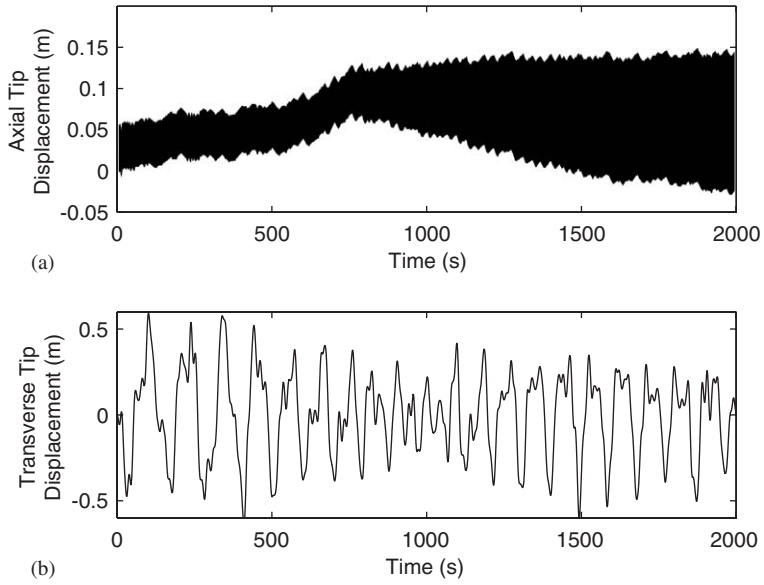

Fig. 16. Axial and transverse tip response to a random wave with significant wave height $H_s = 15$ m and varying end tension: (a) axial tip displacement, (b) transverse tip displacement.

amplitude, and ω is the frequency of parametric excitation. The results are analyzed for the significant wave height $H_s = 15$ m.

Figs. 18 and 19 show the range of responses to a range of forcing frequencies. The forcing frequency is varied from 6 to 15 rad/s in increments of 3 rad/s. As can be seen from the figures, only the axial response is affected by changing the external forcing frequency. There seems to be little effect on the magnitude and shape of the transverse response of the beam due to changes in the forcing frequency. Increasing the frequency though tends to decrease the amplitude of heave response.

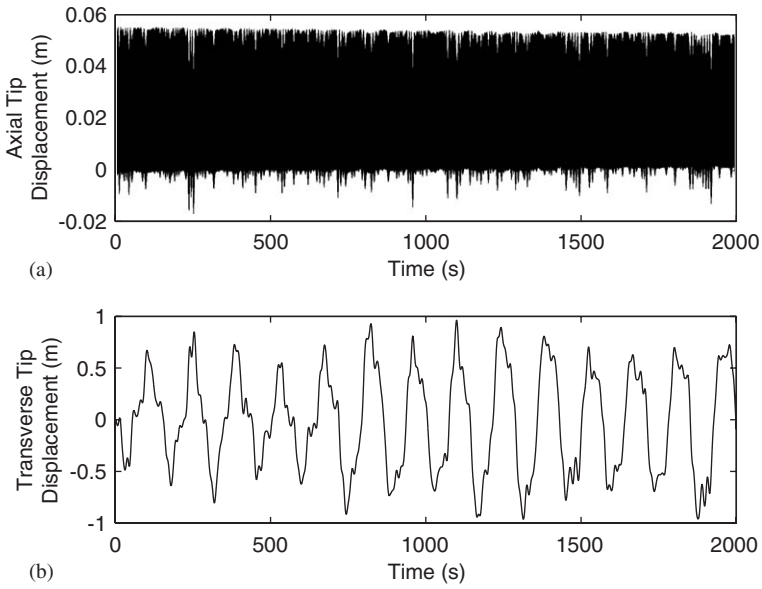

Fig. 17. Axial and transverse tip response to a random wave with significant wave height $H_s = 15\,\text{m}$ and constant end tension of 1252.5 tons: (a) axial tip displacement, (b) transverse tip displacement.

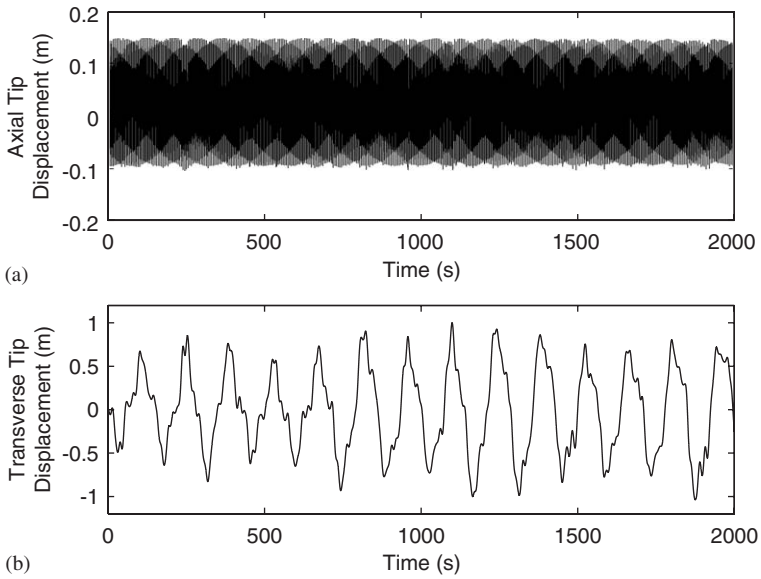

Fig. 18. Axial and transverse tip response of the tether for an axial forcing frequency of $\omega = 6\,\text{rad/s}$: (a) axial tip displacement, (b) transverse tip displacement.

5. Conclusions

A 1.27 m beam model subjected to various end tension is analyzed. Next the response of a 260 m tether with constant end tension subjected to random wave loading is analyzed. Increasing the significant wave height increases the amplitude of transverse response v whereas the amplitude of axial response is not affected appreciably. The axial response u is mainly due to elongation and, as the end tension is kept constant, it does

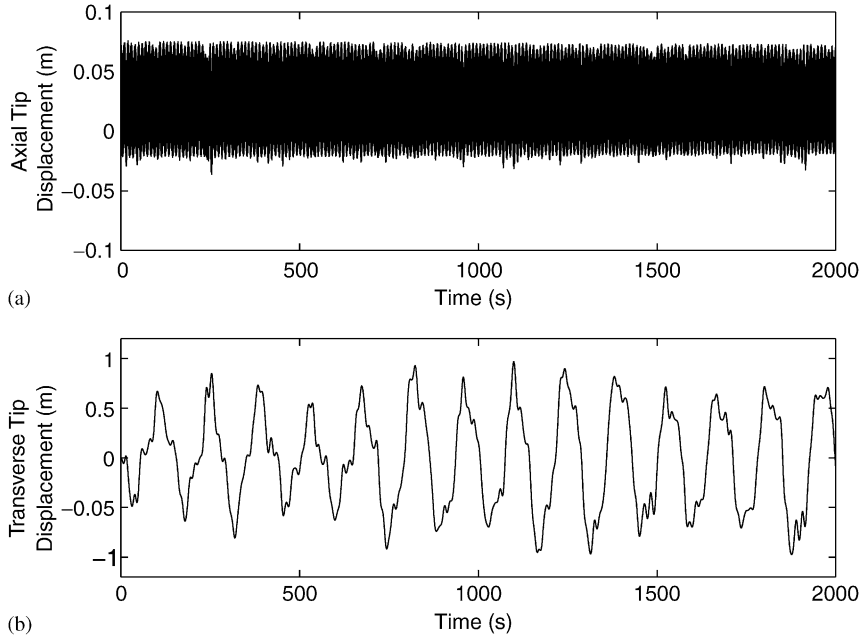

Fig. 19. Axial and transverse tip response of the tether for an axial forcing frequency of $\omega = 15\,\text{rad/s}$: (a) axial tip displacement, (b) transverse tip displacement.

not change significantly. The stress in the tower increases with the increase in significant wave height due to increased transverse displacement.

The effect of increasing the end tension is investigated and the following observations were drawn:

- At zero end tension, the axial displacement is negative, as it is induced geometrically due to transverse motion. Increase in tension causes elongation and produces a positive axial displacement. The absolute value of total maximum axial displacement initially decreases when the end tension is increased from zero to 1562.5 tons, but starts to increase with further increase in end tension.
- The transverse response of the tower with no end tension increases with time. Introducing an end tension stabilizes the transverse response and also decreases the amplitude of displacement initially. At very high end tensions the amplitude of transverse response increases slightly.
- The bending stress in the tether decreases due to lesser transverse displacement as the end tension increases but the total stress in the tether initially decreases and then increases with increase in end tension due to large axial stresses.
- The power spectral density plots show peaks at higher frequencies with increase in tether tension.

It was observed that when the end tension is varied, the magnitude of maximum transverse tip displacement is reduced when compared to the transverse displacement of a tether with constant end tension. Also there is considerable increase in the magnitude of the axial displacement in the case of varying end tension.

It was observed that as the axial forcing frequency is increased, only the axial response is affected. The transverse response remains about the same. Thus it can be concluded that the surge amplitude is not affected by the nonlinearity due to varying axial forces.

Acknowledgments

This work was supported by the Office of Naval Research Grant no. 14-97-1-0017. We would like to thank our program manager Dr. Thomas Swean for his interest and financial support. Also, we appreciate the

detailed improvements offered us by the diligent reviewers. The first author would like to thank Professor Seon M. Han for her early assistance.

References

[1] The International Society of Offshore and Polar Engineers, *Design Considerations for TLP Risers in Harsh Environment*, Cameron Offshore Engineering Limited, Woking, UK, 1991.
[2] A. Bokaian, Natural frequencies of beams under compressive axial loads, *Journal of Sound and Vibration* 126 (1) (1988) 49–65.
[3] A. Bokaian, Natural frequencies of beams under tensile axial loads, *Journal of Sound and Vibration* 142 (3) (1990) 481–489.
[4] Y. Luo, Frequency analysis of infinite continuous beams under axial loads, *Journal of Sound and Vibration* 213 (5) (1998) 791–800.
[5] A.K. Jain, Nonlinear coupled response of offshore tension leg platforms to regular wave forces, *Ocean Engineering* 24 (7) (1997) 577–592.
[6] S. Ahmad, Stochastic TLP response under long crested random sea, *Computers and Structures* 61 (6) (1996) 975–993.
[7] K. Takahashi, Y. Konishi, Non-linear vibrations of cables in three dimensions—part 1: non-linear free vibrations, *Journal of Sound and Vibration* 118 (1) (1987) 69–84.
[8] M.S. Triantafyllou, C.T. Howell, Dynamic response of cables under negative tension: an ill-posed problem, *Journal of Sound and Vibration* 174 (4) (1994) 433–447.
[9] L.N. Virgin, R.H. Plaut, Effect of axial loads on forced vibrations of beams, *Journal of Sound and Vibration* 168 (9) (1993) 395–405.
[10] G. Xie, Y. Dong, J.Y.K. Lou, Stability of vortex-induced oscillations of tension leg platform tether, *Ocean Engineering* 19 (6) (1992) 555–571.
[11] S.M. Han, H. Benaroya, Three dimensional vibration of a compliant tower, *Journal of Sound and Vibration* 250 (4) (2002) 675–709.
[12] S.M. Han, H. Benaroya, Comparison of linear and nonlinear responses of a compliant tower to random wave forces, *Chaos, Solitons and Franctals* 14 (2) (2002) 269–291.
[13] B.B. Mekha, Implications of tendon modeling on nonlinear response of TLP, *Journal of Structural Engineering* 122 (2) (1996) 142–149.
[14] M.H. Patel, H.I. Park, Combined axial and lateral responses of tensioned buoyant platform tethers, *Engineering Structures* 17 (10) (1995) 687–695.
[15] M.H. Patel, H.I. Park, Dynamics of tension leg platform tethers at low tension—part 1: Mathieu stability at large parameters, *Marine Structures* 4 (1991) 257–273.
[16] M.H. Patel, H.I. Park, Tensioned buoyant platform tether response to short duration tension loss, *Marine Structures* 8 (1995) 543–553.
[17] S.M. Han, H. Benaroya, Nonlinear coupled transverse and axial vibration of a compliant structure 1: formulation and free vibration, *Journal of Sound and Vibration* 237 (5) (2000) 837–873.
[18] S.M. Han, H. Benaroya, Nonlinear coupled transverse and axial vibration of a compliant structure 2: forced vibration, *Journal of Sound and Vibration* 237 (5) (2000) 874–899.
[19] H. Benaroya, *Mechanical Vibration*, Prentice-Hall, Englewood Cliffs, NJ, 1998.
[20] W. Weaver, S. Timoshenko, D. Young, *Vibration Problems in Engineering*, Wiley, New York, 1990.
[21] L. Meirovitch, *Analytical Methods in Vibrations*, Macmillan, New York, 1967.
[22] J. Wilson, *Dynamics of Offshore Structures*, Wiley, New York, 1984.
[23] S. Chakrabarti, *Hydrodynamics of Offshore Structures*, Computational Mechanics Publications, 1987.
[24] S.M. Han, H. Benaroya, *Nonlinear and Stochastic Dynamics of Compliant Offshore Structure*, Kluwer Academic Publishers, Dordrecht, The Netherlands, 2002.
[25] A.S. Yigit, A.P. Christoforou, Coupled axial and transverse vibrations of oilwell drillstrings, *Journal of Sound and Vibration* 195 (4) (1996) 617–627.
[26] Joint Industry Project, Guidelines for offshore structural reliability analysis. Technical Report 95-3198, Det Norske Veritas, 1996. http://research.dnv.com/skj/offguide/TLP-Eks.pdf